

Thermo-Responsive Actuation of a DNA Origami Flexor

Vladimir A. Turek, Rohit Chikkaraddy, Sean Cormier, Bill Stockham, Tao Ding, Ulrich F. Keyser,* and Jeremy J. Baumberg*

Nanomachines capable of controlled programmable work at the nanoscale promise to revolutionize a vast range of research and eventually should impact on daily lives. Due to the ease of design and modification, DNA origami is emerging as a natural platform to build such machines. However, one essential challenge is the controlled and rapid actuation of DNA origami using an external biocompatible stimulus. Here, actuation based on temperature-induced phase transitions of the thermo-responsive polymer poly(*N*-isopropylacrylamide) (PNIPAM) is reported. By incorporating this polymer into DNA origami structures on either side of a flexible region, a “DNA origami flexor” is created that uses the tunable PNIPAM hydrophobicity to reversibly open and close the DNA structures. Such a mechanism has the advantage of being versatile and biocompatible, and possessing strong response to temperature changes of a few degrees Kelvin.

1. Introduction

DNA nanotechnology enables unprecedented control on the nanoscale.^[1,2] It has become possible to construct arbitrary predefined nanoarchitectures of ever increasing complexity through a relatively simple design process^[3] based on DNA origami (DNAo) which folds a single long biological “scaffold” with many short synthetic “staples.”^[4,5] The conceptual simplicity of DNAo together with computer-aided design^[6] and the vast potential for controlled nanoarchitecture has resulted in an explosion of research interest.^[7] This bottom-up approach now attains levels of precision for nanoconstructs that exceed those of top-down techniques.^[8,9]

Although DNAo is a successful self-assembling technique evidencing potential to revolutionize applications that require control of matter on the nanoscale, DNAo implementations are hindered by the difficulty of creating reusable machinery that actuates rapidly and efficiently. Recyclable nanomachines

or enzymes built from DNAo which carry out preprogrammed work^[2] are of great interest for their nanocatalytic potential, which would justify their cost. Akin to biological enzymes, such nanomachines could capture several components, bring them into proximity, react them together, and release them ready for the cycle to be repeated. Such systems require rapid, controlled, reversible conformational changes in the DNAo in order to facilitate these processes.

One of the most common strategies for conformational changes in DNAo has been “DNA fuel”—the introduction of staples that hybridize to single-stranded components in the origami and therefore change the shape the DNAo has to

adopt.^[3,5,10–12] Reversibility can be achieved by the subsequent removal of these staples by additional strands that are more complementary to the first staple than the origami. Although the DNA fuel approach demonstrates that origami actuation is possible in a remarkably precise manner (on sub-nm scales),^[11] there are numerous drawbacks. Aside from the fact that any change in conformation requires a modification to the chemical composition of the surrounding solution, this method is also slow (each cycle takes minutes), generates waste strands, making each cycle successively harder to pump, and requires difficult additional design considerations (such as the presence of a single-stranded region that upon hybridization creates enough strain in the DNAo to induce a conformational change). The slow response time (of minutes to hours) is a major drawback of origami nanoactuators, unavoidably leading to forces which are small compared with thermal forces and unable to move around structural components such as nanoparticles.

Faster actuation mechanisms are thus demanded. Alternative actuation triggers have included pH/ions,^[10,13,14] hydrophobicity,^[15] or electric potentials.^[16] However, the state-of-the-art to date has been UV light-triggered systems,^[13,17] which make use of *cis*–*trans* isomerization between azobenzene derivatives. These have the advantage of being fast, controllably reversible, externally triggered and unlike electrochemical actuation do not need to be tethered to a surface. Despite these benefits of azobenzene-based actuation over DNA fuel, the bleaching of azobenzene limits the number of cycles that such nanomachines can undergo, while the forces produced remain too small. They also introduce complex design considerations for conformational changes, and require UV light, which is generally undesirable for many applications, making this a less-than-perfect actuation mechanism.

Dr. V. A. Turek, R. Chikkaraddy, S. Cormier, B. Stockham, Prof. T. Ding, Prof. U. F. Keyser, Prof. J. J. Baumberg
NanoPhotonics Centre
Cavendish Laboratory
University of Cambridge
Cambridge CB3 0HE, UK
E-mail: ufk20@cam.ac.uk; jjb12@cam.ac.uk

Prof. T. Ding
School of Physics and Technology
Wuhan University
Wuhan 430072, China

 The ORCID identification number(s) for the author(s) of this article can be found under <https://doi.org/10.1002/adfm.201706410>.

DOI: 10.1002/adfm.201706410

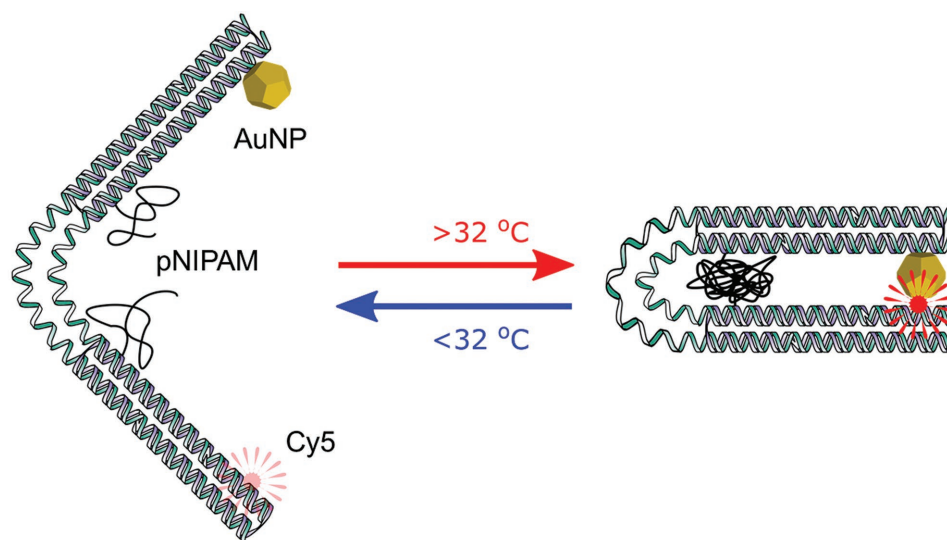


Figure 1. Schematic of DNAo flexor. Above the LCST, the PNIPAM chains on both sides of the hinge become hydrophobic, causing the two arms of origami to fold due to hydrophobic interactions. Once the temperature is lowered below the LCST, PNIPAM rehydrates thereby unfolding the origami structure. A gold nanoparticle and fluorescent molecule are fixed on opposite ends of the plate DNAo to give optical responses to its actuation.

Recently, the thermo-responsive properties of poly(*N*-isopropylacrylamide) (PNIPAM) have been demonstrated as a fast and powerful actuation mechanism for the manipulation of nanoparticles.^[18] Such actuation is extremely attractive as it utilizes a convenient external stimulus which can be delivered either by light, by heating, or through chemical changes, while being biocompatible. The properties of PNIPAM have been studied extensively since the late 1960s.^[19] The mechanism for the phase transition involves hydrogen bonding in the backbone of the polymer that becomes unfavorable above $T_c = 32\text{ }^\circ\text{C}$ causing an increase in its hydrophobicity and a coil-to-globule transition as the polymer rearranges to minimize its contact with water. The transition is accompanied by a significant change in the volume of polymer. The ratio of gyration/hydration radii, R_g/R_h , goes from ≈ 1.5 (a random coil in good solvent) at room temperature to less than $(3/5)^{1/2}$ (a uniform hard sphere which is smaller) above T_c .^[20] Understanding this mechanism has enabled researchers to tune the lower critical solution temperature (LCST, T_c) by incorporation of PNIPAM into block copolymers or adjusting the solvent composition, allowing this to match physiologically relevant temperatures.^[21]

Here, we introduce an improved DNAo actuation mechanism that makes use of the phase transition of PNIPAM. By incorporating PNIPAM-modified staples on either side of a flexible hinge, a plate-like DNAo is reversibly opened or closed with temperature changes of a few Kelvin (**Figure 1**). In order to monitor the DNAo flexor in real time, a gold nanoparticle and a fluorescent molecule are fixed on opposite ends of the plate structures, giving an optical response upon actuation. The advantages of this actuation method are the convenience of using rapid temperature control, the full reversibility of the actuation without photobleaching, the efficacy of incorporating PNIPAM into DNAo designs, and the versatility to tune the actuation in many ways. Furthermore, actuators based on PNIPAM have the potential to provide large forces ($>n\text{N}$) as well as show fast switching rates (μs or faster);^[18,22] however,

further experiments are needed to quantify these in the DNAo flexor.

2. Results and Discussion

2.1. PNIPAM–DNA Conjugation

Despite the natural synergy between smart polymers and DNAo for actuation purposes, surprisingly only a single work details the use of PNIPAM with DNAo, aiming rather differently to create reversible giant surfactants.^[23] This work used copper-catalyzed azide-alkyne cycloaddition (CuAAC) to form a PNIPAM–DNA block copolymer which can then be used as a regular staple strand to fold origami. While the general “click chemistry” route is one of the most convenient to tether DNA to polymers (due to biocompatibility and a near perfect yield), CuAAC tends to be limited by the disproportionation reaction of the Cu(I) catalyst. This can be countered by using accelerating and stabilizing ligands such as tris(1,2,3-triazolyl)methylamine in conjunction with ascorbate to reduce any oxidized Cu(II) back to the active Cu(I) form.^[24]

As a favorable alternative,^[25] a catalyst-free strain promoted azide-alkyne cycloaddition (spAAC) is instead employed here (**Figure 2a**). By incorporating the alkyne into a highly strained eight-membered ring (dibenzocyclooctyne-DBCO) into the staple sequence with an azide-terminated PNIPAM derivative, the cycloaddition proceeds to completion at ambient conditions (Figure 2b). spAAC has the added benefit of being compatible with aqueous environments, and requires only the azide and alkyne conjugates for the reaction meaning fewer purification steps compared with CuAAC.

2.2. DNAo Design

The nanomachine test platform for this actuation mechanism is a modified two-layer plate design used by Hemmig et al.^[9]

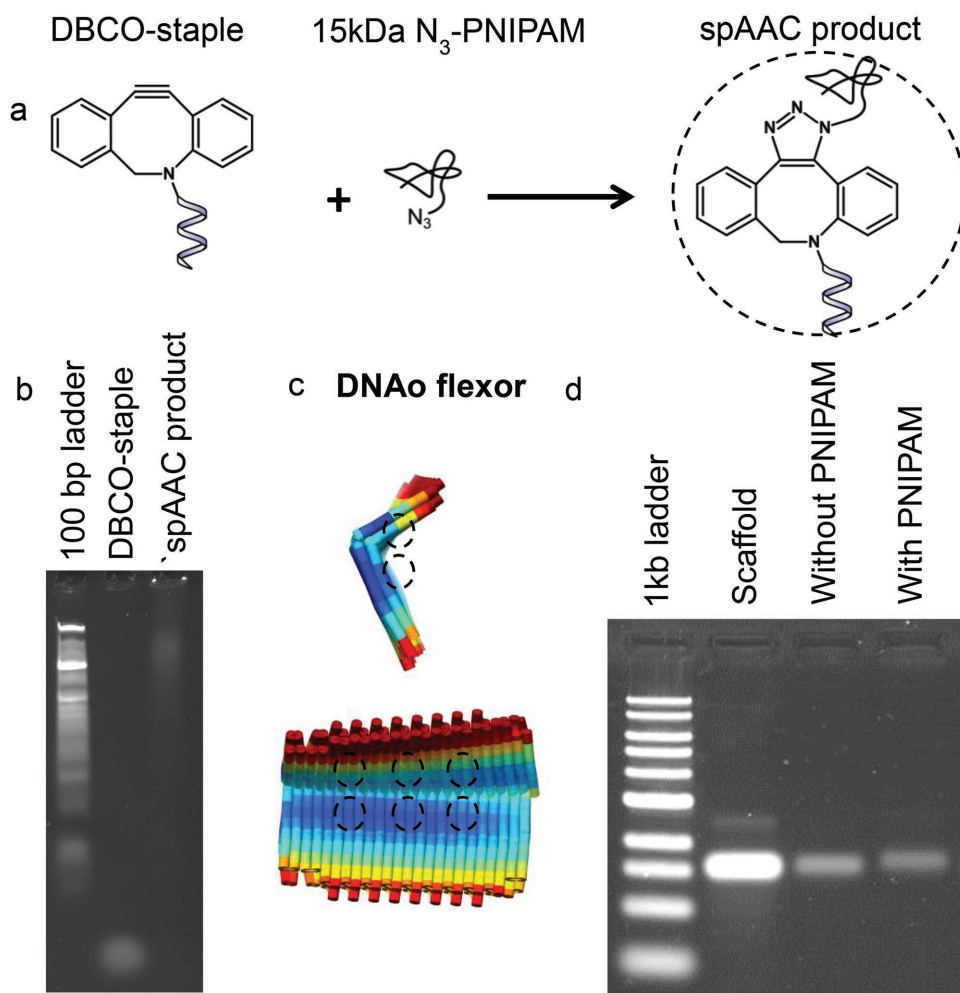


Figure 2. Reaction scheme, design, and characterization of the origami. a) PNIPAM–DNA staple preparation to form the DBCO-staple azide-terminated PNIPAM strand using strain-promoted azide-alkyne cycloaddition (spAAC). b) Polyacrylamide gel electrophoresis of unmodified and modified DNA staples shows 100% conversion. c) Snapshot of DNAo flexor structure from simulation (CanDo) showing PNIPAM sites (dashed circles). d) Agarose gel electrophoresis of PNIPAM-functionalized DNAo shows $3.1 \pm 0.1\%$ reduced electrophoretic mobility over unfunctionalized DNAo.

By simply omitting two columns of staples in the caDNAno design (Figure S1, Supporting Information), a flexible hinge is created between two rigid arms (Figure 2c). Three overhangs containing the PNIPAM–DNA copolymer are then hybridized into the origami on either side of the hinge. At room temperature, the two arms have a random orientation with respect to each other. However, once the temperature is elevated above $32\text{ }^{\circ}\text{C}$, the increased hydrophobicity of the PNIPAM closes the arms as soon as the two PNIPAM sites find each other. The difference in the conformations between the cold and hot states (i.e., random and fixed configurations, respectively) of the origami causes a difference in the mobility of the origami. This is seen in agarose gels run at $45\text{ }^{\circ}\text{C}$ (Figure 2d) which show a $3.1 \pm 0.1\%$ decrease in electrophoretic mobility of the DNAo containing PNIPAM compared with designs without the PNIPAM–DNA copolymer. This difference might be attributed to mass differences between the two designs, as the six PNIPAM–DNA copolymers ($\approx 120\text{ kDa}$) adds $\approx 2\%$ to the total mass of the origami ($\approx 5000\text{ kDa}$). Slower electrophoretic

migration of DNA structures which incorporate hydrophobic moieties has also been reported elsewhere.^[15]

Atomic force microscopy (AFM) is performed in a $50 \times 10^{-3}\text{ M}$ MgCl_2 $0.5\times$ tris base, acetic acid and EDTA (TAE) buffer on the folded origami (Figure S2a,b, Supporting Information) to characterize the assembly. Aside from the clear presence of the hinge due to the omitted staples, it is also evident that most of the origamis are deposited in the open state. This is not unexpected since there are attractive van der Waals forces between the mica and DNA, as well as repulsive electrostatic DNA–DNA interactions. A small minority of structures do nevertheless appear closed—due to the high ionic strength of the buffer, electrostatic screening allows some of the origami structures to shut. This observation of closed structures in AFM shows that the hinge is flexible enough to let the arms to lock in place if the hydrophobic effects of collapsed PNIPAM are strong enough. Careful deposition of the DNA flexors in the closed state can also be imaged in AFM when dried (Figure S2c, Supporting Information), showing the clear change in morphology.

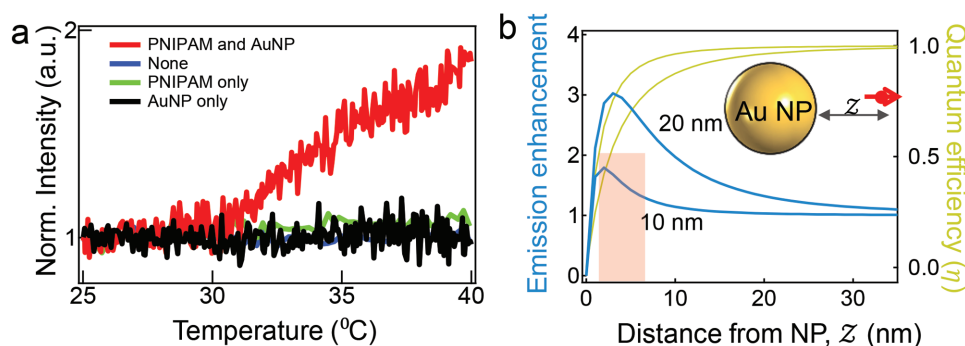


Figure 3. Surface-enhanced fluorescence of PNIPAM-actuated DNAo. a) Interaction between Cy5 and 16 nm Au NP placed on opposite arms of the DNA flexor. During closure, an increased emission intensity (red) is seen, which is absent when the PNIPAM or NP are omitted (blue, green, and black). b) FDTD simulations of point dipole emitter approaching Au NP also show that emission enhancement and quantum efficiency depend also on nanoparticle size ($2R = 10\text{--}20$ nm). Observed doubling of emission implies distance between NP and dye drops to 3–7 nm.

2.3. Surface-Enhanced Fluorescence

To determine whether mobility changes are due to PNIPAM-driven actuation of the origami above T_c , the origami is modified to include a small (16 nm diameter) gold nanoparticle (Au NP) on one arm and a dye (Cy5) on the other arm in the equivalent position. Energy transfer between the Cy5 and the Au NP controls the Cy5 emission efficiency which strongly dependent on their separation (Figure 3b). The fluorescence intensity is found to increase by 90% when heated to 40 °C (Figure 3a) but only when the DNAo is functionalized with all three modifications (PNIPAM, Cy5, and Au NP). This increase in emission is not seen when either the PNIPAM strands or the particle is omitted; however, a small 10% increase is seen when the PNIPAM strands alone are included. The actuation-induced emission enhancement is corroborated by Finite-difference time-domain (FDTD) simulations. Normalized emission intensities are calculated for different distances of Cy5 (modeled as a classical point dipole with internal quantum efficiency of 20%) from the Au. For NP diameters of 10–20 nm, the emission enhancement of ≈ 2 is obtained when the distance between Cy5 and Au NP drops to 3–7 nm. In the open state, based on simple geometric arguments, the separation between the dye and the Au NP will randomly fluctuate between 0 and ≈ 26 nm, with a mean separation of ≈ 17 nm. At the “average separation” therefore, the surface-enhanced fluorescence effect will be negligible. More accurate quantification of this distance is obscured by additional contributions from increased scattering as the origami conformation changes as well as changes in the chemical environment of the dye in the closed state. Indeed, the control for DNAo with PNIPAM but without the NP (green curve in Figure 3a) shows a 10% increase in emission above 32 °C, presumably due to this increased scattering cross-section of the closed state.

2.4. Dynamic Light Scattering

Further evidence of the thermal responsive behavior of the system comes from dynamic light scattering (DLS) measurements (Figure 4). Though the mass and volume of the DNAo do not change with increasing temperature (at least prior to onset

of significant DNA melting at 55 °C, Figure S3, Supporting Information), DLS measurements show a dramatic change in mobility between the hot and cold states. Counterintuitively, an increased effective size is observed for the closed DNA flexor despite its lower surface area. This difference in mobility heralds the change of conformation in line with the changes observed in the gels (Figure 2d). To discuss this, we first note that the elasticity of the flexor plates in the open state will lead to a distribution of conformations and therefore a larger distribution in the sizes that DLS records. By contrast, in the closed state, there is only one conformation and a much narrower DLS distribution is observed. The sizes that DLS reports for these samples have little physical significance however, since DLS is only valid for spheres and the origami is plate-like.

For 2×10^{-3} M MgCl_2 in the absence of PNIPAM (Figure 4a), there is a gradual increase in the DLS size of the origami as a function of temperature, from 60 nm at 25 °C to 68 nm at 40 °C with a corresponding increase in polydispersity index (PDI) of 0.30 to 0.39. In the presence of PNIPAM however (Figure 4b), an initial gradual increase in size up to 30 °C is followed by a dramatic change at the LCST of PNIPAM: from 61 nm at 25 °C (PDI 0.37) and 63 nm at 30 °C (PDI 0.20) to 170 nm at 32 °C (PDI 0.08) and 282 nm at 40 °C (PDI 0.12). The continued growth above 32 °C in 2×10^{-3} M MgCl_2 is likely due to dimer formation between the DNAo flexors, due to strong repulsion between the phosphate backbones at such low ionic strength. This makes the closed state kinetically favorable at 32 °C but the dimers thermodynamically favorable at 40 °C. For intermediate ionic strengths of 11×10^{-3} M MgCl_2 (Figure 4c), the apparent size increases from 72 ± 2 nm (PDI 0.31 ± 0.03) to 114 ± 1 nm (PDI 0.07 ± 0.01) when heating from 25 to 40 °C. Under these conditions, dimerization of the origami does not occur in either the cold or the hot states, because electrostatic repulsion is sufficiently screened to allow the hinge to close, but not enough to enable nonspecific aggregation of the base pairs. At higher ionic strengths of 20×10^{-3} M MgCl_2 (Figure 4d), the closed state at 40 °C is still similar to the 11×10^{-3} M MgCl_2 case (though with lower effective size of 105 ± 4 nm from more screening), but a bimodal distribution is seen at 25 °C. This is due to the nonspecific aggregation of the origami, which are however only weak bound and easily broken up by the PNIPAM-actuated closing.

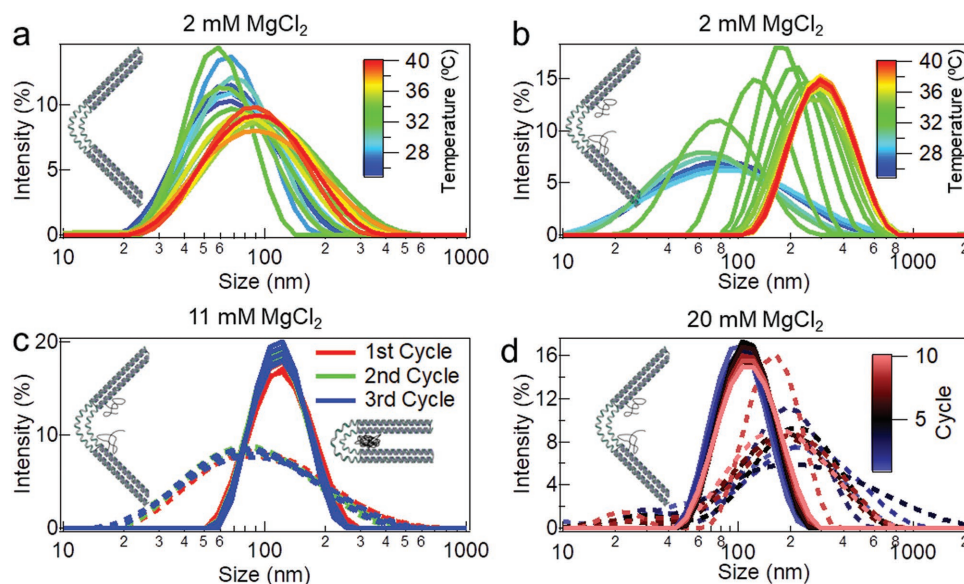


Figure 4. DLS from cycling DNA flexor between open and closed states. a) DNAo flexor without PNIPAM shows only gradual change in effective DLS size with temperature (2×10^{-3} M MgCl_2). b) DNAo flexor with PNIPAM gives clear transition above 32°C due to PNIPAM collapse and closing of the flexor, increasing effective size and narrowing distribution (2×10^{-3} M MgCl_2). c) At 11×10^{-3} M MgCl_2 , repeated cycling confirms increased size in closed state with narrower size distribution. d) At 20×10^{-3} M MgCl_2 , the cold state appears larger due to formation of aggregates between the origamis; however, these aggregates are broken up at 40°C and the closed flexor remains unchanged after multiple cycles, despite differences in the aggregated open state (solid lines 40°C , dashed 25°C).

The DLS results suggest that in the closed state, the DNA flexor diffusion coefficient is smaller than in the open state. This is surprising given that the larger effective surface area of the open-state origami should increase friction with water, slowing it down. Hydrodynamic calculations (WinHydroPRO)^[26] however support the hypothesis that the open structure should have a smaller translation diffusion coefficient (Figure S7, Supporting Information). To verify that the features seen in DLS are indeed from opening–closing of the DNA flexor, the PNIPAM mechanism was substituted by an established “chemical fuel” mechanism using hydrophobic interactions of cholesterol, which also gives rise to both the narrowed DLS size distribution and a larger apparent size (Figure S4, Supporting Information). Further controls were performed by utilizing a different, single-layer cholesterol-actuated “chemical fuel” design from List et al.^[15] (Figure S6, Supporting Information). While the size distribution of this design did not change as much as with the DNA flexor design (likely due to the greater flexibility of the one-layer plate), the apparent size increase with the cholesterol strands present is clear. We thus conclude that such changes in DLS are indeed characteristic of actuation of our DNAo flexor. Further investigations to establish the precise cause for this counter-intuitive result are ongoing.

The results here clearly demonstrate the reversible actuation of a DNAo flexor. While further experiments are required to determine the rates and forces involved in the cycling actuation mechanism, previous work suggests PNIPAM-based actuators possess both fast switching rates (μs) and high stress (nN).^[18,22] It is worth noting that aside from PNIPAM, other polymers can be incorporated into DNAo in a similar fashion to alter the trigger mechanism and potentially even enhance the specificity of the actuation mechanism.^[27] The ability to induce

conformational changes in DNAo using such a direct actuation mechanism opens exciting avenues to design nanomachines and robots that carry out preprogrammed functions. One such function could be in bringing together two target molecules followed by their reaction together, a type of synthetic DNA enzyme. Further, temporary covalent attachment of the molecules to the arms of the DNAo flexor would naturally constrain their orientation—such a system would be a practical demonstration of “mechanosynthesis.”

3. Conclusions

We have demonstrated a thermo-responsive actuating DNA nanomachine based on the hydrophobic phase transition at the LCST of PNIPAM. This actuation mechanism has the advantage of being easy to incorporate into DNAo designs, having an external, biocompatible, and tuneable stimulus, and in principle being fast and delivering powerful actuation forces (the quantification of which is ongoing). This work opens avenues for the intelligent design of nanomachines with a preprogrammed function for uses in drug delivery, sensing, catalysis, and controlled manipulation of matter at the nanoscale using bottom-up methods. Such actuation is a key step toward the design and construction of entirely artificial DNA-based “enzymes” for fast, efficient, and controlled assembly of nanomaterials.

4. Experimental Section

DNAo was designed using caDNAo software. Unmodified staples were purchased from Integrated DNA technologies. The cholesterol-modified

staple and the dibenzocyclooctyne (DBCO)-modified staple were purchased from Biomers. Azide-terminated PNIPAM (average M_n 15 000, PDI \leq 1.3) was purchased from Sigma Aldrich. For the DNA flexor, a p7560 scaffold was used, while for the design published by List et al a p7249 scaffold (M13mp18) was used, both purchased from tilibit nanosystems.^[15] All water used in solution was ultrapure (MilliQ, with resistivity of 18.2 M Ω cm).

PNIPAM–DNA Conjugation: A 3'-modified DBCO staple (AAAATAAAATAAAATAAAAT) (50×10^{-6} M) was left to react with N₃-terminated PNIPAM (0.5×10^{-3} M) in water at room temperature for at least 1 d prior to use (though the reaction seemed to proceed to completion <1 h). The mixture was left unpurified and added to the staple mix for folding (the subsequent filtration of the folded origami through the membrane acted to remove the excess unbound PNIPAM).

Nanoparticle Synthesis: Au NPs with a 16 nm diameter were prepared using the standard Turkevich method, using 8.62 mg HAuCl₄ · 3H₂O dissolved in 95 mL water heated to reflux, followed by the addition of 20 mg sodium citrate tribasic dihydrate in 5 mL water. The reaction proceeded by the characteristic pale yellow to colorless to black to purple to ruby red within a period of 5 min, and the solution was left to reflux for a further 15 min following this, before cooled to room temperature under stirring. The size of the particles was characterized by scanning electron microscopy.

Origami Folding: Staples were mixed together to a concentration of 200×10^{-9} M from the initial 100×10^{-6} M in a 1 \times TE buffer pH 8 to form the master mix. In a polymerase chain reaction (PCR) tube, 20 μ L of this solution was added to 4 μ L (100×10^{-9} M) of the scaffold with 8.4 μ L of water, 2 μ L 10 \times TE buffer, and 5.6 μ L 100×10^{-3} M MgCl₂ to yield a folding mixture consisting of 14×10^{-3} M MgCl₂, 1 \times TE. The origami in the PCR tube was then folded by raising the temperature of the mixture to 90 °C, followed by a gradual cooling to room temperature over a period of 23 h, followed by a holding temperature of 4 °C. Each tube was then filtering through a 100 kDa Amicon filter unit using a 2×10^{-3} M MgCl₂, 0.5 \times TBE washing buffer using 3–5 centrifugation cycles.

FDTD Simulation: The 3D numerical simulations were performed using Lumerical FDTD Solutions v8.12. The Au NP was modeled as a sphere of different diameters (10–20 nm) in a water medium of refractive index 1.33. The dielectric function of gold was taken from Johnson and Christy.^[28] The nanoparticle was illuminated with a broad band plane wave (total-field scattered-field (TFSF) source) from inbuilt source parameter of wavelengths ranging from 500 to 900 nm. The field profile monitor was used to record the near-field electric field enhancements around the nanoparticle (E/E_0).

Further to calculate the quantum yield and the enhancement/suppression of light emission from the fluorophore, the plane wave source was replaced by an electric dipole source. The distance between the nanoparticle surface and dipole was varied to map the quantum efficiency while fixing the dipole axis perpendicular to the nanoparticle surface.

The emission enhancement (γ_{em}) was estimated from combining the enhancements in near-field intensity (E^2/E_0^2) and quantum efficiency (η) as $\gamma_{em} = (E^2/E_0^2) \times (\eta/\eta_0)$. This takes into account the internal quantum efficiency (η_0) of the Cy5 20%.

Supporting Information

Supporting Information is available from the Wiley Online Library or from the author. Source data can be found at: <https://doi.org/10.17863/CAM.20705>.

Acknowledgements

The authors acknowledge financial support from UK EPSRC Grants EP/G060649/1, EP/L015978/1, and EP/L027151/1, NanoDTC, and ERC Grant LINASS320503. R.C. acknowledges support from the Dr. Manmohan Singh scholarship from St. John's College.

Conflict of Interest

The authors declare no conflict of interest.

Keywords

DNA origami, dynamic light scattering, nanomachines, surface-enhanced fluorescence, thermo-responsive polymers

Received: November 3, 2017

Revised: February 2, 2018

Published online:

- [1] a) A. Krissanaprasit, M. Madsen, J. B. Knudsen, D. Gudnason, W. Surareungchai, V. Birkedal, K. V. Gothelf, *ACS Nano* **2016**, *10*, 2243; b) X. Ouyang, M. De Stefano, A. Krissanaprasit, A. L. B. Kodal, C. B. Rosen, T. Liu, S. Helmig, C. Fan, K. V. Gothelf, *Angew. Chem., Int. Ed.* **2017**, *56*, 14423.
- [2] R. K. O'Reilly, A. J. Turberfield, T. R. Wilks, *Acc. Chem. Res.* **2017**, *50*, 2496.
- [3] E. S. Andersen, M. Dong, M. M. Nielsen, K. Jahn, R. Subramani, W. Mamdouh, M. M. Golas, B. Sander, H. Stark, C. L. Oliveira, *Nature* **2009**, *459*, 73.
- [4] a) N. C. Seeman, *J. Theor. Biol.* **1982**, *99*, 237; b) J. Chen, N. C. Seeman, *Nature* **1991**, *350*, 631; c) H. Yan, X. Zhang, Z. Shen, N. C. Seeman, *Nature* **2002**, *415*, 62; d) P. Yin, H. Yan, X. G. Daniell, A. J. Turberfield, J. H. Reif, *Angew. Chem., Int. Ed.* **2004**, *43*, 4906; e) P. W. Rothmund, *Nature* **2006**, *440*, 297.
- [5] a) B. Yurke, A. J. Turberfield, A. P. Mills, F. C. Simmel, J. L. Neumann, *Nature* **2000**, *406*, 605; b) A. J. Turberfield, J. Mitchell, B. Yurke, A. P. Mills Jr., M. Blakey, F. C. Simmel, *Phys. Rev. Lett.* **2003**, *90*, 118102.
- [6] S. M. Douglas, A. H. Marblestone, S. Teerapittayanon, A. Vazquez, G. M. Church, W. M. Shih, *Nucleic Acids Res.* **2009**, *37*, 5001.
- [7] a) C. Steinhauer, R. Jungmann, T. L. Sobey, F. C. Simmel, P. Tinnefeld, *Angew. Chem., Int. Ed.* **2009**, *48*, 8870; b) N. A. Bell, U. F. Keyser, *FEBS Lett.* **2014**, *588*, 3564; c) S. Hernández-Ainsa, N. A. Bell, V. V. Thacker, K. Göpfrich, K. Misiunas, M. E. Fuentes-Perez, F. Moreno-Herrero, U. F. Keyser, *ACS Nano* **2013**, *7*, 6024; d) Q. Zhang, Q. Jiang, N. Li, L. Dai, Q. Liu, L. Song, J. Wang, Y. Li, J. Tian, B. Ding, *ACS Nano* **2014**, *8*, 6633.
- [8] a) N. V. Voigt, T. Tørring, A. Rotaru, M. F. Jacobsen, J. B. Ravnsbæk, R. Subramani, W. Mamdouh, J. Kjems, A. Mokhir, F. Besenbacher, *Nat. Nanotechnol.* **2010**, *5*, 200; b) A. Gopinath, E. Miyazono, A. Faraon, P. W. Rothmund, *Nature* **2016**, *535*, 401; c) V. V. Thacker, L. O. Herrmann, D. O. Sigle, T. Zhang, T. Liedl, J. J. Baumberg, U. F. Keyser, *Nat. Commun.* **2015**, *5*, 3448.
- [9] E. A. Hemmig, C. Creatore, B. Wünsch, L. Hecker, P. Mair, M. A. Parker, S. Emmott, P. Tinnefeld, U. F. Keyser, A. W. Chin, *Nano Lett.* **2016**, *16*, 2369.
- [10] Y. Ke, T. Meyer, W. M. Shih, G. Bellot, *Nat. Commun.* **2016**, *7*, 10935.
- [11] A. E. Marras, L. Zhou, H.-J. Su, C. E. Castro, *Proc. Natl. Acad. Sci. U. S. A.* **2015**, *112*, 713.
- [12] a) M. Marini, L. Piantanida, R. Musetti, A. Bek, M. Dong, F. Besenbacher, M. Lazzarino, G. Firrao, *Nano Lett.* **2011**, *11*, 5449; b) L. Piantanida, D. Naumenko, E. Torelli, M. Marini, D. M. Bauer, L. Fruk, G. Firrao, M. Lazzarino, *Chem. Commun.* **2015**, *51*, 4789; c) A. Kuzuya, Y. Sakai, T. Yamazaki, Y. Xu, M. Korniyama, *Nat. Commun.* **2011**, *2*, 449.

- [13] S. Hernández-Ainsa, M. Ricci, L. Hilton, A. Aviñó, R. Eritja, U. F. Keyser, *Nano Lett.* **2016**, *16*, 4462.
- [14] D. Liu, S. Balasubramanian, *Angew. Chem., Int. Ed.* **2003**, *42*, 5734.
- [15] J. List, M. Weber, F. C. Simmel, *Angew. Chem., Int. Ed.* **2014**, *53*, 4236.
- [16] S. Hernández-Ainsa, K. Misiunas, V. V. Thacker, E. A. Hemmig, U. F. Keyser, *Nano Lett.* **2014**, *14*, 1270.
- [17] a) Y. Yang, M. Endo, K. Hidaka, H. Sugiyama, *J. Am. Chem. Soc.* **2012**, *134*, 20645; b) Q. Jiang, Q. Liu, Y. Shi, Z.-G. Wang, P. Zhan, J. Liu, C. Liu, H. Wang, X. Shi, L. Zhang, J. Sun, B. Ding, M. Liu, *Nano Lett.* **2017**, *17*, 7125.
- [18] T. Ding, V. K. Valev, A. R. Salmon, C. J. Forman, S. K. Smoukov, O. A. Scherman, D. Frenkel, J. J. Baumberg, *Proc. Natl. Acad. Sci. U. S. A.* **2016**, *113*, 5503.
- [19] M. Heskins, J. E. Guillet, *J. Macromol. Sci., Chem.* **1968**, *2*, 1441.
- [20] C. Wu, X. Wang, *Phys. Rev. Lett.* **1998**, *80*, 4092.
- [21] a) U. Rauwald, J. del Barrio, X. J. Loh, O. A. Scherman, *Chem. Commun.* **2011**, *47*, 6000; b) S. Li, Y. Su, M. Dan, W. Zhang, *Polym. Chem.* **2014**, *5*, 1219.
- [22] a) S. Murphy, S. Jaber, C. Ritchie, M. Karg, P. Mulvaney, *Langmuir* **2016**, *32*, 12497; b) Z. Qian, D. S. Ginger, *J. Am. Chem. Soc.* **2017**, *139*, 5266.
- [23] T. R. Wilks, J. Bath, J. W. de Vries, J. E. Raymond, A. Herrmann, A. J. Turberfield, R. K. O'Reilly, *ACS Nano* **2013**, *7*, 8561.
- [24] J. E. Hein, V. V. Fokin, *Chem. Soc. Rev.* **2010**, *39*, 1302.
- [25] C. R. Becer, R. Hoogenboom, U. S. Schubert, *Angew. Chem., Int. Ed.* **2009**, *48*, 4900.
- [26] A. Ortega, D. Amorós, J. G. de La Torre, *Biophys. J.* **2011**, *101*, 892.
- [27] a) P. J. M. Stals, M. A. J. Gillissen, R. Nicolaÿ, A. R. A. Palmans, E. W. Meijer, *Polym. Chem.* **2013**, *4*, 2584; b) A. K. Sharma, M. Caricato, E. Quartarone, S. Edizer, A. G. Schieroni, R. Mendichi, D. Pasini, *Polym. Bull.* **2012**, *69*, 911.
- [28] P. B. Johnson, R. W. Christy, *Phys. Rev. B* **1972**, *6*, 4370.